04

Investigation of high-frequency pulsed discharge in air using high-speed video recording

© N.A. Sharapov,[1] S.E. Malanichev,[1] V.Y. Traubergs,[1,2] A.S. Belev,[1,2] D.V. Korepin[2]

[1] Bauman Moscow State Technical University,
105005 Moscow, Russia
[2] LLC „UF PULS“,
[2] 603155 Nizhny Novgorod, Russia
E-mail: valtraubergs@gmail.com

Received April 10, 2025
Revised July 8, 2025
Accepted July 20, 2025

This study investigates the dynamics of frequency pulsed discharge in atmospheric pressure air using high-speed video recording. Oscillograms of the discharge current and voltage were analyzed. By correlating the temporal evolution of the discharge, captured in high-speed images, with the data obtained from an oscilloscope, three phases of the discharge process were identified. The experiments were conducted at a pulse repetition rate 1−10 kHz and pulse energy 1−4 mJ. The discharge type was identified, which made it possible to explain for its structural features and formation mechanisms

Keywords: non-equilibrium plasma, pulsed discharge, high-frequency discharge, pulsed arc discharge, discharge dynamics.

DOI: 10.61011/TP.2026.01.62842.58-25

Introduction

Low-temperature plasma is widely applied in various fields of science and technology [1]. It is used in materials science, nanotechnologies, ecology, surface treatment as well as in medicine and biotechnologies. For example, in industry the low-temperature plasma is applied for modifying material properties [2], precision cleaning, which is especially important in microelectronics for removal of organic contaminants, etching substrates and improving adhesion of thin-film coatings [3,4] and in ecology for plasma-chemical decomposition of harmful substances [5]. In medicine, the low-temperature plasma is used for antibacterial treatment, acceleration of tissue healing, tool sterilization and generation of biologically active compounds. One of the examples is synthesis of nitrogen monoxide (NO) in air discharges, such as corona, barrier, arc discharges, etc. [6–9]. Experimental studies have shown that „bulk“ pulsed discharge is the most suitable for generation [10].

The „bulk“ pulsed discharge is understood to be a discharge formed as a set of separated channels that occur sequentially in time and are spatially distributed within a discharge gap. Due to radial diffusion and overlapping of traces of discharge channels, a visual effect is created in camera exposure, at which the discharge occupies a significant volume.

The object of this study is a frequency pulsed discharge in air at atmospheric pressure. It is the discharge that consists of a sequence of pulses repeated with a certain repetition rate. In the previous study [11], we obtained and described a discharge structure and its typical appearance is shown in Fig. 1.

It was found that the discharge was a conducting channel being formed between two electrodes. With each new pulse, the channel is formed in a new place. The timing parameters of discharge excitation are adjusted so that the next pulse is applied only after termination of an active phase. This mode determines a nature of discharge existence. Multiple channels visible in the photos are explained by a high pulse repetition rate and duration of exposure of shooting equipment.

Further advancement of low-temperature plasma technologies requires a detailed study of the mechanisms of discharge formation and evolution.

The present study is aimed at detailed investigation of a unit discharge pulse and description of its dynamics based on frame-accurate analysis of a video record obtained by means of a high-speed camera.

1. Experimental setup description

For detailed investigation of dynamics of a separate pulse, it was decided to switch from the coaxial electrode system described in the study [11] to an axial one, thereby more accurately tracing discharge development. Dynamics of formation and development of the frequency pulsed discharge was studied on a dedicated experimental bench designed to control the pulse repetition rate within the range from 1 to 10 kHz, an atmospheric air flowrate within the range 1−10 l/min and energy imparted to each pulse within 1−4 mJ. Voltage pulses were formed using a pulse generator. The system of the vertical electrodes is fixed in a frame detachable structure made of a plastic using

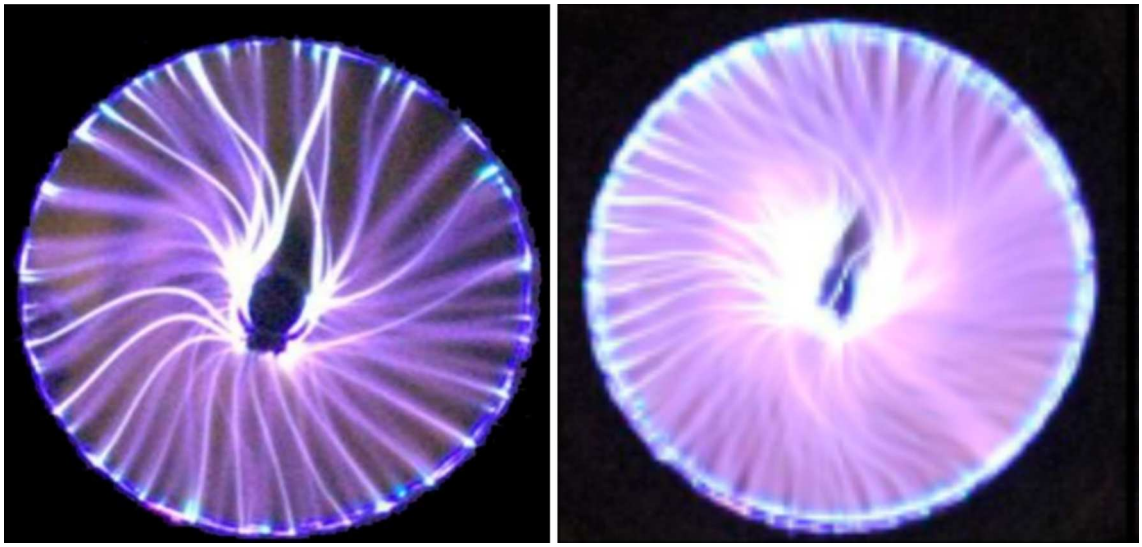

Figure 1. Appearance of the discharge (the pulse repetition rate 1300 Hz and 2800 Hz, respectively, exposure of 1/50 s) [11].

3D-printing technologies, wherein a base is perforated for outflow of a working gas (Fig. 2). A distance between the electrodes is (5 ± 0.1) mm. A material of an upper electrode is brass and that of a lower one is copper.

The discharge process was registered using the high-speed Phantom v2512 camera designed to operate at a frequency of 675 200 frames per second and exposure of 0.97 μs. The camera was placed at a distance of 38 cm from a discharge region.

Voltage at the discharge gap was measured using a capacitive voltage divider, while the current was measured using current sensors. Signals from the divider and the current sensor were supplied to a digital storage oscilloscope AKIP-4122. The measurement unit diagram is shown in Fig. 3.

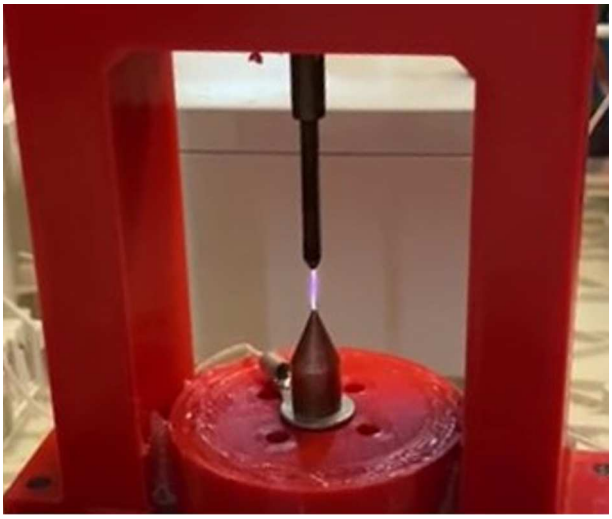

Figure 2. Discharge in the electrode system.

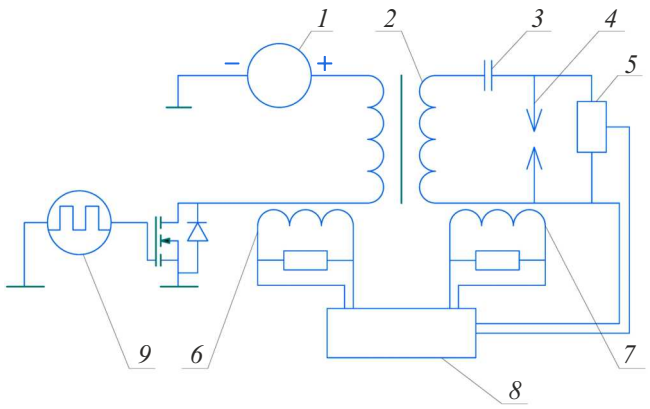

Figure 3. Measurement unit diagram: *1* — the source, *2* — the pulse transformer, *3* — the limiting capacitor, *4* — the electrode system, *5* — the high-voltage probe, *6* — the primary-winding current sensor, *7* — the secondary-winding current sensor, *8* — the registering system, *9* — the pulse oscillator.

Before the experiment was started, the measurement system was calibrated to compensate a systematic error. Voltage division coefficients k_1 and coefficients of proportionality of the current sensor k_2 were determined. As a result, the following values were obtained: $k_1 = 1000$; $k_2 = 1$ A/V. A bandwidth of the capacitive divider was 1 kHz–20 MHz, while a bandwidth of the current sensor was 1 kHz–1 MHz.

Channel sizes cannot be accurately determined without finding a correlation between the obtained images and real sizes. This parameter is determined via a coefficient of proportionality, which is a ratio of a known typical size to its analogue on the image. The typical size was a distance between the electrodes $L = (5 \pm 0.1)$ mm, which was pre-photographed at the same position of the camera relative

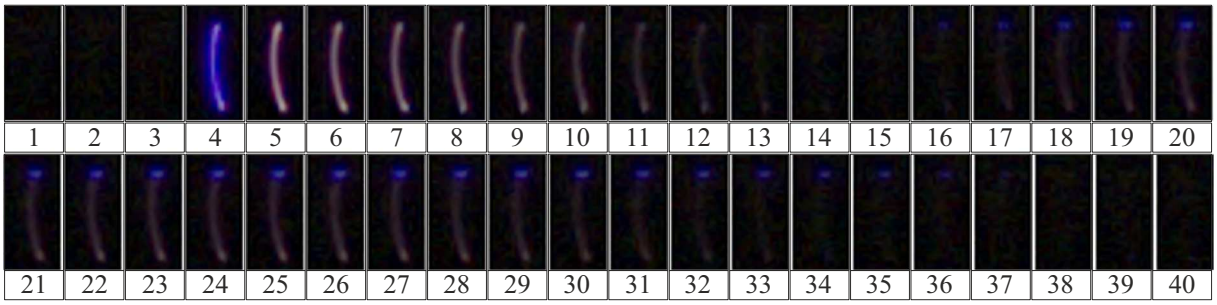

Figure 4. Dynamics of discharge pulse development.

to the bench and with the same resolution. The image was analyzed in the GIMP raster editor to show that the distance between the electrodes in the picture was 25 pixels, which makes it possible to determine a recalculation coefficient: 1 pixel corresponds to 0.2 mm.

2. Experimental results

A typical discharge duration was 50 μs, while time resolution of the used video camera was 1.5 μs, which made it possible to capture the discharge development pattern (Fig. 4).

Image processing included the analysis of a region in direct proximity to the discharge, which had a size of 18×36 (3.6×7.2 mm, respectively).

The level of frame brightness was estimated by frame-accurate analysis of a histogram of the grayscale images. It means that a pixel brightness distribution was analyzed for each frame. Reference values are accepted to be: 100 % — a fully light-exposed (white) image, 0 % — a fully black image. The results are used to plot a graph of a dependence of relative light exposure of frames on time, which reflects variation of discharge brightness at the various stages of its development (Fig. 5).

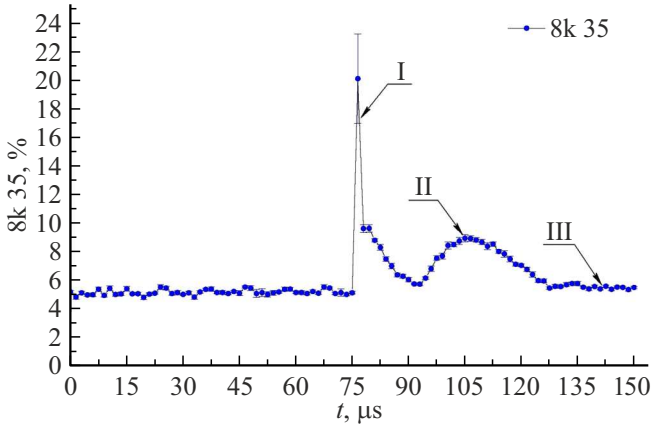

Figure 5. Frame light exposure (percentage): the phase I — formation of the ionization channel, the phase II — energy release, the phase III — deionization.

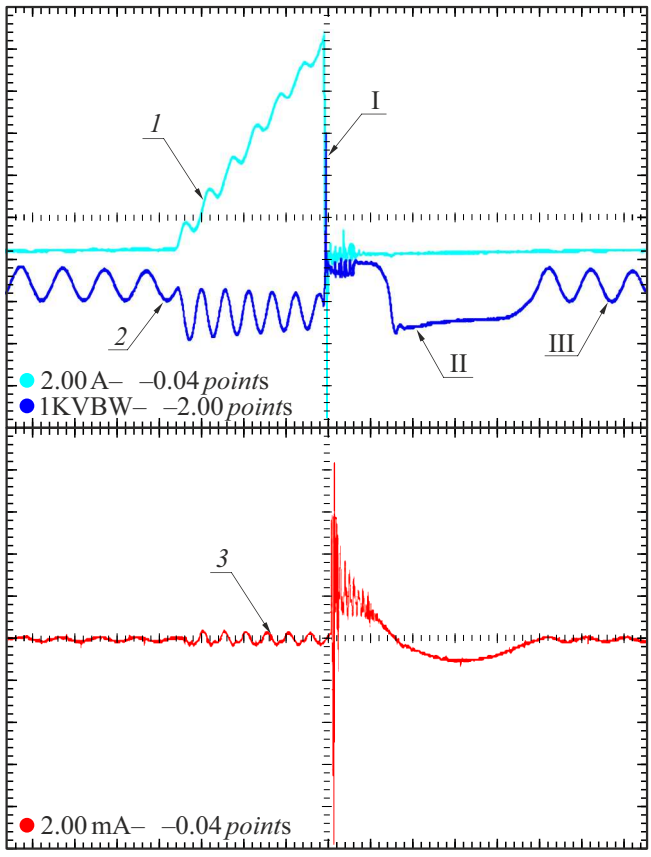

Figure 6. Curve *1* — the oscillogram of the transformer primary-winding current, the curve *2* — the voltage oscillogram, the curve *3* — the oscillogram of the transformer secondary-winding current. The scale is 10 μs. The phase I — formation of the ionization channel, the phase II — energy release, the phase III — deionization.

At the same time, oscillograms of discharge current and voltage were recorded (Fig. 6 — the frequency of 8 kHz, pulse energy — 4 mJ, the flowrate — 10 l/min). They clearly demonstrate discharge development and allow better understanding its specific features. The curve *1* is a form of the primary current waveform, the curve *2* is voltage at the discharge gap, the curve *3* is a form of the discharge current in an experimental model of the device.

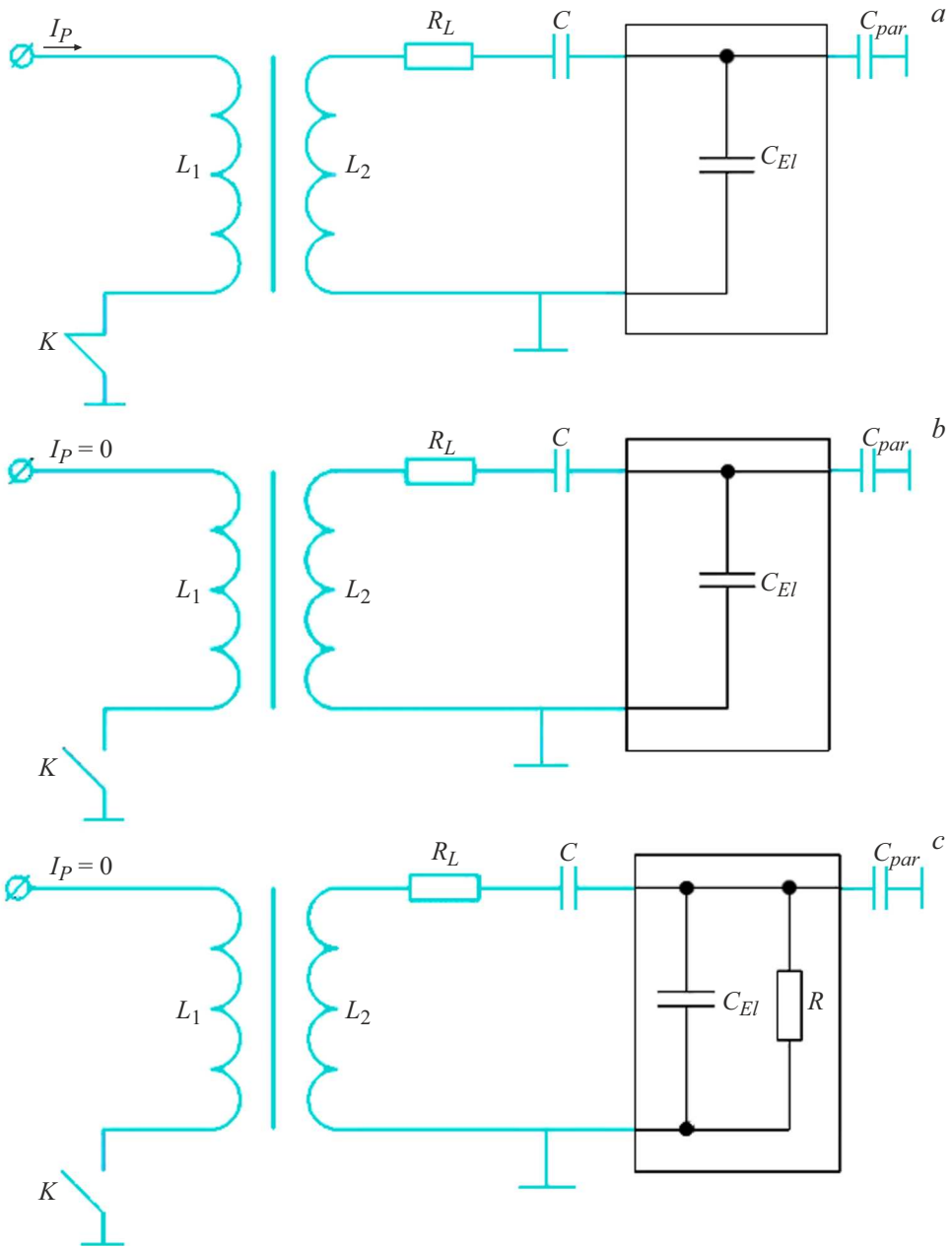

Figure 7. Equivalent electric diagram: *a* — the stage of pumping the circuit with energy, restoration of electrical strength of the gas-discharge gap; *b* — the stage of breakdown of the electrode gap and discharge formation, *c* — the stage of energy release in the discharge; I_P — the pumping current (a current amplitude value), L_1 — the transformer's primary winding, L_2 — the transformer's secondary winding, R_L — the coil resistance, R — the equivalent resistance of the discharge channel, C — the limiting capacitance, C_{par} — the spurious capacitance, C_{El} — the equivalent capacitance of the discharge gap.

One of the key specific features of the pulse discharge is a method of energy input into a discharge volume (circuit) [10]. The operating chamber is an element of an oscillatory circuit with external pulsed excitation, in which energy was released. The connection diagram of the oscillatory circuit is shown in Fig. 7.

As mentioned above, the key feature of this discharge is the method of energy input into the discharge volume. A discharge chamber is an element of the oscillatory circuit, in which energy is input in batches and controlled in each pulse.

An amplitude, form and time characteristics of the discharge current depend on a chamber geometry, parameters of the oscillatory circuit, a gas flowrate and a value of input energy.

Energy was input into the circuit as follows. At the time T_1 (see the equivalent scheme — Fig. 7, *a*) the low-voltage winding of the pulse transformer L_1 is connected

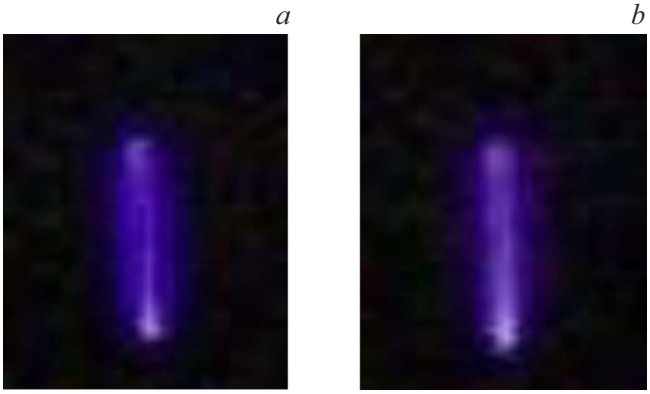

Figure 8. Appearance of the ionization channel.

to a voltage source. At the same time, the current via it smoothly increases to a certain value (the current amplitude determines a value of energy input into the discharge). There is no current in the secondary winding L_2 since induced voltage at the secondary winding (a voltage level is determined by a transformation coefficient of the pulse transformer) is not enough for breakdown of an electrode gap. Then, at the time T_2, the switch is opened.

Generally, not all energy stored in an inductance element will be input into the discharge, since losses are unavoidable in a core, an ohmic resistance of the transformer windings and electromagnetic radiation of the system.

The next stage (the phase I — Fig. 6) of the process will occur at the moment of opening an electronic key in the primary network of the diagram. Synchronously, polarity of voltages changes at the secondary side of the pulse transformer and its level sharply increases. At this time, there is no discharge, since its active resistance is infinite and the system is a series resonant circuit , which produces voltage resonance at the discharge gap. The circuit (see the equivalent scheme — Fig. 7, *b*) originates high-frequency current oscillations at the background of the applied high-voltage pulse voltage and there is a breakdown of the electrode gap.

Thus, the discharge is a high-frequency breakdown in the volume. The current amplitude and the oscillation frequency are determined by elements of the circuit diagram and also affect preliminary ionization of a medium.

The breakdown (preliminary ionization of the medium) is just followed by the next stage — the discharge formation stage (the phase II — Fig. 6). As it is known, a self-sustained volume discharge of high (atmospheric) pressure is non-stationary, i.e. after some time it contracts and

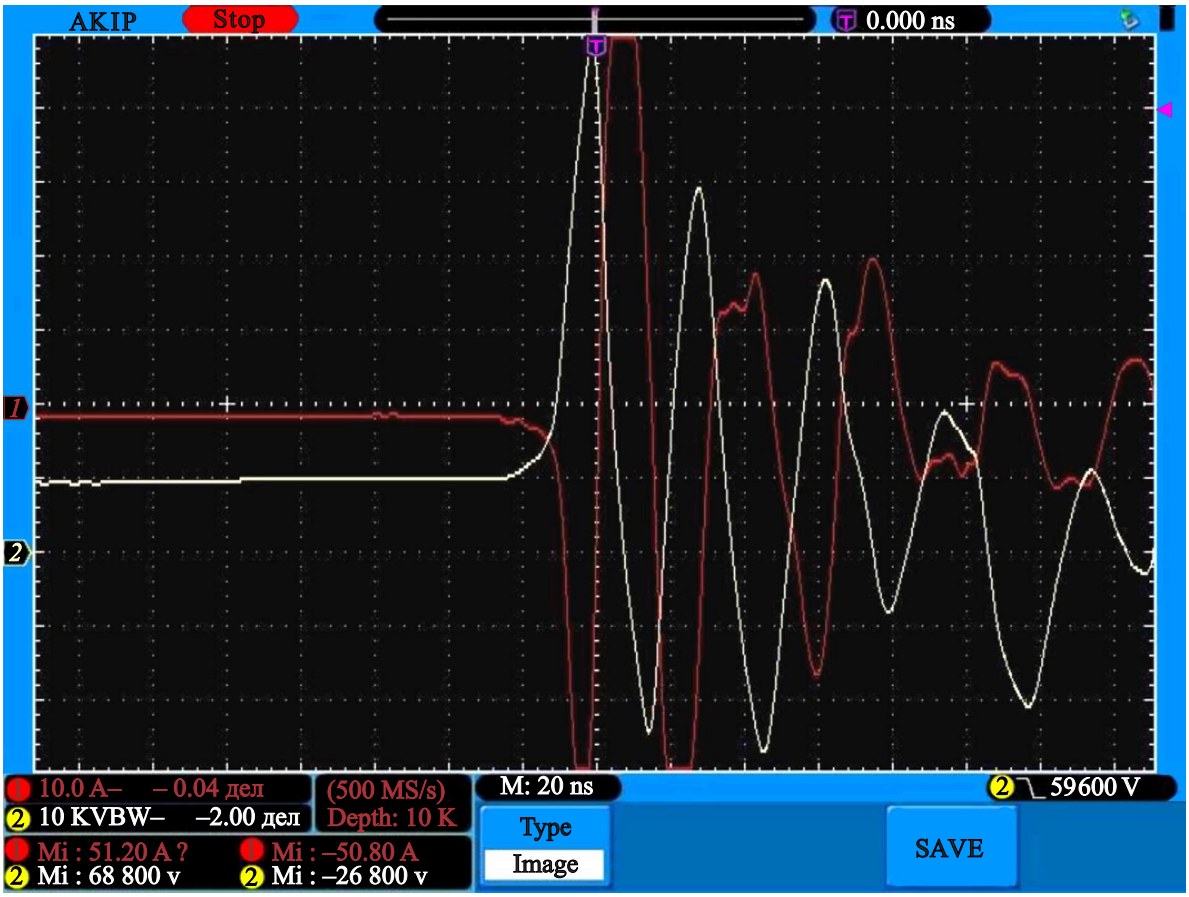

Figure 9. Oscillograms of voltage at the pulse transformer output winding (the curve *2*) and HF current oscillations in a reactor network (the curve *1*).

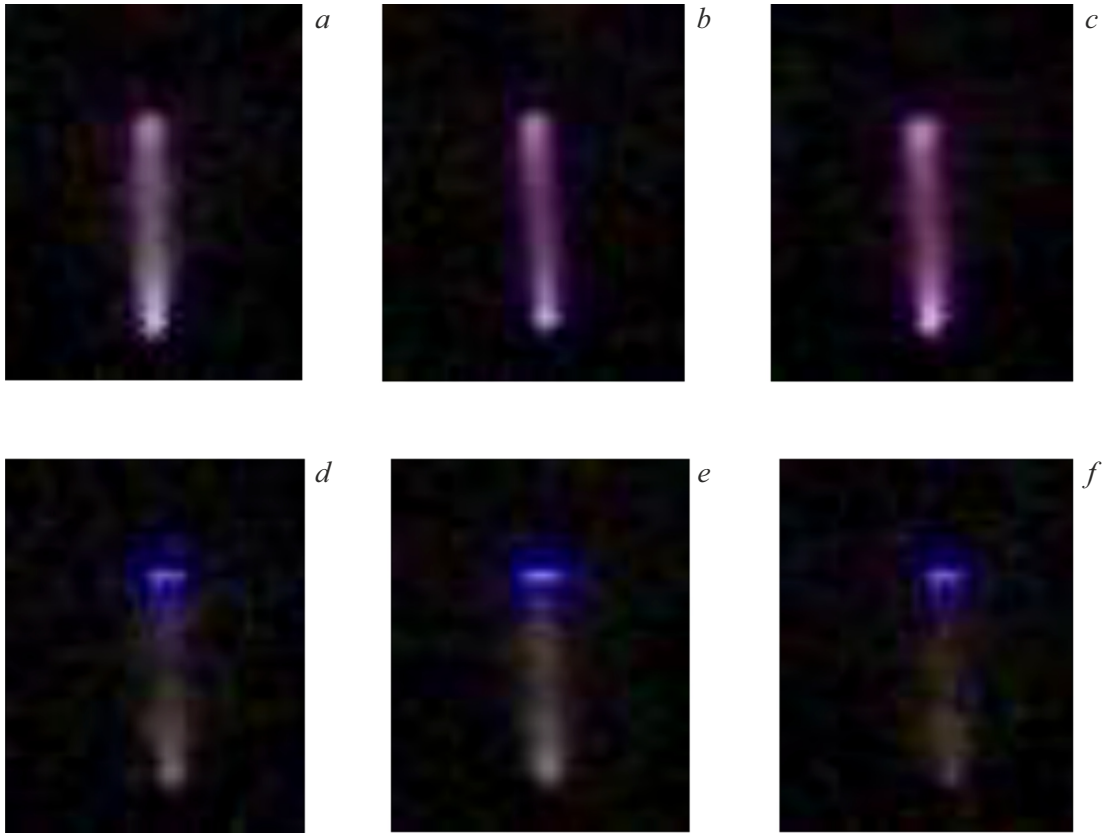

Figure 10. Appearance of the discharge at the stage of energy release: $a-c$ — the first half-wave, $d-f$ — the second half-wave.

transitions into an arc discharge. It is believed that the main input of energy into the gas is at this stage (it corresponds to the energy input phase in our case, (Fig. 7, *c*), and a maximum amount of energy input into the discharge also depends on energy spent for preliminary ionization and this dependence is of a linear nature.

Analysis of discharge development at the obtained photos and their comparison with the oscillogram made it possible to select three phases of the discharge process: preliminary ionization, energy release in the channel and deionization.

The first phase (I, Fig. 6) corresponds to formation of the ionization channel shown in Fig. 8. At the initial moment of time there is no discharge and active resistance of the medium is infinite. The oscillatory circuit with a reactor is excited at the resonance frequency (20−40 MHz) with a voltage amplitude of up to 50 kV. In the formed high-frequency field, the medium in the electrode gap is ionized (the process duration is $1-2\,\mu$s). The channel geometry is determined by the frequency and amplitude of the HF current flowing through the discharge gap (Fig. 8).

In order to explain a mechanism of the first phase, Fig. 9 shows an oscillogram of the HF current flowing through the discharge gap in this phase (the curve *1*), at an artificial simulated mode of breakdown absence. This mode was created by increasing the discharge gap between the electrodes above a voltage breakdown threshold.

At this stage, the gas in the discharge gap is ionized throughout the volume, thereby resulting in an avalanche-like increase of a concentration of electrons in the discharge gap. As soon as the concentration of electrons reaches a critical value, the second phase of discharge starts (II, Fig. 6). The second phase is characterized by formation of the conducting channel with finite resistance, thereby resulting in the change of the parameters of the oscillatory circuit and release of energy stored therein. The current amplitude is determined by a wave resistance: reactive resistance of induction and capacitance as well as active resistance of the discharge.

As a result, the frequency of the current oscillations decreases by several orders and is determined by parameters of elements included in the oscillatory circuit. A typical appearance of the discharge at the stage of energy release is shown in Fig. 10.

The third phase (III, Fig. 6) includes deionization of the channel. At this stage, the discharge current ceases and resistance of the discharge gap sharply increases. The oscillatory circuit returns to a state that is similar to the stage of preliminary ionization. The remaining energy in the circuit excites HF oscillations that are similar to the first portion.

3. Determination of the discharge geometry

As noted above, the plasma parameters in the operating chamber can be determined via a geometry of the discharge channel. The highest interest is paid to a plasma state in the first two phases, especially at the stage of preliminary ionization.

For analysis, diameters of the discharge channel in Fig. 8 (the phase I) and 10 (the phase II) have been measured. Taking into account the coefficient of proportionality $k = 0.0684$, the following values of the average diameters of the discharge channel have been obtained:

Phase I: $d_1^{\mathrm{I}} = 0.08\,\mathrm{mm}$, $d_2^{\mathrm{I}} = 0.068\,\mathrm{mm}$, where d_1^{I}, d_2^{I} is an average diameter of the channels in Fig. 8, *a, b*, respectively.

Phase II: d_1^{II}=0.089 mm, d_2^{II}=0.084 mm, d_3^{II}=0.064 mm, where d_1^{II}, d_2^{II}, d_3^{II} — an average diameter of the channels in Fig. 10, $a-c$, respectively.

Conclusion

The present study involved investigation of a time structure of the frequency pulsed discharge with the pulse repetition rate from 1 to 10 kHz and pulse energy within the range 1−4 mJ in air at atmospheric pressure and recording the oscillograms of the discharge current and voltage of the discharge gap. The oscillogram was analyzed together with the discharge dynamics to show that the discharge process consisted of three stages, i.e. formation of the ionization channel in the HF field, the phase of energy release and deionization of the medium. Based on high-speed images, the diameters of the discharge channels were measured at the first two stages (I and II), which made it possible to obtain quantitative characteristics of their development.

Based on the obtained data, it is planned in the further studies to calculate the key plasma parameters at each stage of formation and evolution of the discharge, which will allow describing mechanisms of its development in greater detail.

Acknowledgments

The authors would like to thank Department SM-4 of Bauman Moscow State Technical University represented by chief V.V. Selivanov (Doctor of Technical Sciences) and technical employees N.D. Galina and D.A. Lysov for their high-speed shooting of the experiments.

The authors would like to sincerely thank the company LLC „UF PULSE“ for assistance and support in preparing the article.

Conflict of interest

The authors declare that they have no conflict of interest.

References

[1] Yu.S. Akishev. Izv. vuzov. Kihimiya i khim. tekhnologiya, **62** (8), (in Russian). 26 (2019). DOI: 10.6060/ivkkt.20196208.5908
[2] G. Borcia, N.M.D. Brown. J. Phys. D: Appl. Phys., **40** (7), 1927 (2007). DOI: 10.1088/0022-3727/40/7/015
[3] R. Deltschew, D. Hirsch, H. Neumann, T. Herzog, K.J. Wolter, M. Nowottnick, K. Wittke. Plasma Treatment for Fluxless Soldering, **142**−**144**, 803 (2001). DOI: 10.1016/s0257-8972(01)01181-1
[4] G. Takyi, N.N. Ekere. Soldering Surface Mount Technol., **22** (2), 37 (2010). DOI: 10.1108/09540911011036271
[5] E.S.M. Mouele, J.O. Tijani, O.O. Fatoba, L.F. Petrik. Environmental Science and Pollution Research, **22** (23), 18345 (2015). DOI: 10.1007/s11356-015-5386-6
[6] G. Sathiamoorthy, S. Kalyana, W.C. Finney, R.J. Clark, B.R. Locke. Ind. Eng. Chem. Res., **38** (5), 1844 (1999).
[7] Y. Qi, H. Hu, C. Weipeng, X. Jie, Z. Jinli, W. Shuang. Plasma Sci. Technol., **13** (6), 702 (2011).
[8] K. Heuer, M.A. Hoffmanns, E. Demir, S. Baldus, Ch.M. Volkmar, M. Röhle, P.C. Fuchs, P. Awakowicz, Ch.V. Suschek, Ch. Opländer. Nitric Oxide: Biol. Chem., **44**, 52 (2015). DOI: 10.1016/j.niox.2014.11.015.PMID: 25435001
[9] H. Hu, H. Liang, J. Li, Q. Zhao, J. He. IEEE Transactions on Plasma Sci., **35** (3), 619 (2007). DOI: 10.1109/TPS.2007.896782
[10] N.A. Sharapov, V.I. Chukanov, R.R. Distanov, N.P. Kozlov, A.V. Pekshev, V.A. Khomenko, A.B. Vagapov, R.R. Dusalieva. Inzh. zhurn: nauka i innovatsii, **10** (22), 32 (2013) (in Russian).
[11] N.A. Sharapov, A.A. Khinkis, S.I. Gadzhikhalilova, T.V. Mel'nik, A.V. Parfenov. VANT. Ser. Termoyadernyi sintez, **40** (2), 61 (2017) (in Russian).

Translated by M.Shevelev